The University of
Nottingham

UNITED KINGDOM · CHINA · MALAYSIA

Zacharzewski, Piotr and Jefferson-Loveday, Richard J. and Morvan, Herve (2017) SAS – SST simulations of the flow and heat transfer inside a square ribbed duct with artificial forcing. In: 23rd ISABE Conference, 3-8 Sep 2017, Manchester, UK.

SAS – SST simulations of the flow and heat transfer inside a square ribbed duct with artificial forcing

Piotr Zacharzewski, Richard Jefferson-Loveday and Hervé Morvan
Contact Richard.Jefferson-Loveday@nottingham.ac.uk

Gas Turbine and Transmissions Research Centre (G2TRC)
University of Nottingham
Faculty of Engineering
Nottingham
United Kingdom
NG7 2RD

ABSTRACT

Scale Resolving Simulations (SRS) are emerging as a promising compromise of cost and accuracy for industrial simulations of flows inside turbine blade cooling systems as they represent a necessary increase of accuracy with respect to Reynolds Averaged Navier Stokes (RANS) in the field. In this paper, several hybrid RANS-LES (Large Eddy Simulation) and SRS approaches are investigated. A Scale Adaptive Simulation (SAS) with spectrally calibrated artificial forcing is used to simulate flow inside a development section of a square duct with eight square equispaced ribs.

Energy spectra, two-point correlations as well as other standard metrics are used to assess resolved content qualitatively as well as quantitatively. It is found that unmodified SST-SAS offers a marginal improvement over Unsteady RANS (URANS) for the present type of flow even on a LES-type grid and the solution is essentially steady.

The artificial forcing used seems to trigger the resolving capability of the model and the solution is noticeably closer to experimental results while requiring minor extra computational demand. Effects of rotation are examined and it is found that the rotation appears to trigger the resolving mode of the unforced SAS model.

Keywords: Scale Adaptive Simulation; SST – SAS; square ribbed duct; artificial forcing; Hybrid RANS-LES;

NOMENCLATURE

B. C.	Boundary Condition(s)
C	SAS model constant, 0.11
C_F	Q criterion constant, 0.5
DES	Detached Eddy Simulation
D_h, L	Reference hydraulic diameter, 0.149 [m]
$F_{,i}$	Forcing source term
k	Turbulence Kinetic Energy per unit mass (TKE) $[m^2 s^{-2}]$
LES	Large Eddy Simulation
L_t, L	Modelled turbulence length scale [m]
L_{vK}	Von Karman length scale [m]
N	Numer of harmonic modes, 100
Nu_0	Reference Nusselt number
Pr	Prandtl number
RANS	Reynolds Averaged Navier Stokes
$R_{AB}(\vec{r})$	Normalised correlation coefficient
Ro	Rotation number
S	Strain rate $[s^{-1}]$
SAS	Scale Adaptive Simulation
SRS	Scale Resolving Simulation
SST	Shear Stress Transport
URANS	Unsteady RANS
VM	Vortex Method
Δh	Maximum cell extent [m]
Δt	Timestep $[s^{-1}]$
u'	Fluctuating velocity component in x direction $[m\ s^{-1}]$
$\bar{u}, \bar{u}_{in}$	Mean, or bulk velocity $[m\ s^{-1}]$
$u_{f,i}$	Forcing velocity
ε_{ijk}	Permutation symbol, Levi - Cita
$\eta_i^n, \xi_i^n, d_i^n, \omega^n$	Random numbers from normal distribution
κ	Von Karman constant, 0.41
$\vec{r}$	Relative displacement vector [m]
V	Vorticity $[s^{-1}]$
τ_t	Turbulence time scale [s]
ρ	Density, kg/m^{-3}
σ_φ	SAS model constant, 2/3
γ	Turbulent Kinetic Energy ratio
Ω	Rotational speed $[rad\ s^{-1}]$
ω	Specific dissipation rate $[s^{-1}]$
ζ_2	SAS model constant, 1.47
$\overrightarrow{x_A}$	Absolute displacement vector of point A [m]

1.0   INTRODUCTION

In the era where global air traffic is expected to double in 15 years and continue to increase [1] the efficiency of aeroengines is under immense scrutiny. An area of the aeroengine that can yield significant efficiency gains given a fixed investment is the high pressure turbine, with specific focus on internal cooling [2]. Improved cooling of the turbine blades allows higher turbine entry temperature, and less bleed from other parts of the engine.

Previous studies have shown that RANS or URANS models are inaccurate for predicting flow and heat transfer [3], [4] in aerospace applications and there is an increasing move towards hybrid RANS – LES models in the field [5] [6] [7], especially for internal flows. Presently the reason LES is not employed more widely is its prohibitive computational cost for industrial geometries and flow conditions.

Detached Eddy Simulation (DES) is proposed to remedy the strict LES grid requirements however as a hybrid RANS-LES model it suffers from phenomenon known as grey areas. SAS, devised by Menter et. el. [8] is a variant of the SRS approach that proposes to remedy the problem of DES grey areas and generalise on the concepts by triggering resolving mode based on flow unsteadiness, measured by the Von Karman length scale.

Effectively, this way, steady regions are treated with URANS while unsteady regions are treated with LES and a smooth and natural transition happens at the interface without users' interference or prior knowledge of the flow. The model reverts to URANS even in unsteady regions if the grid is unsuitable.

The SAS model however was found to be lacking resolved content even on geometries that are well known to be unsteady and strongly separated such as an axisymmetric hill [9] or sharp edged rib [10]. It was found that the resolving mode is not triggered even under those strongly turbulent conditions. To remedy the problem, Menter et. al. proposed artificial forcing [11] to trigger the 'LES' like behaviour of the SST – SAS model. The forcing is based on ideas of Kraichnan et. al.. [12], Smirnov [13] and Batten [14] and was proven to work for a reverse-facing step [11]. Forcing will be discussed in more detail later.

1.1   Previous works

Due to cost limitations, RANS remains the workhorse of the industrial engineering community for turbine blade design. Complex, engine realistic geometries are analysed with this technique by Dhopade et. al. [15] and Gillespie et. al. [16] and a difference of up to 25% with respect to experimental results is found. For a somewhat more simplified geometry investigated numerically as well as experimentally by Schuler et. al. [17] [18] it was found that differences up to 20% can be seen with standard RANS $k - \omega$ modelling approach.

With respect to the present geometry, Sewall et. al. performed experiments [19] as well as LES calculations [20]. Viswanathan et. al. [21] performed DES simulations on the geometry and further inflow sensitivity and more insights on LES is provided by Tyacke and Tucker [3]. It was found that LES results are in excellent agreement with experimental data. The Detached Eddy Simulation of Viswanathan performs slightly worse than LES but still significantly better than any RANS model studied both in terms of flow and heat transfer.

Simpler square ribs using the present flow conditions were studied by Liu [22] and Ooi and Iaccarino et. al. [23], again primarily with RANS models or hybrid approaches on RANS – like grids. The present authors also studied SST – SAS on square ribbed channel using the periodic conditions [10]. It was found that SST-SAS solution is similar to RANS and with significant difference from experiment.

Similar flow conditions and geometries were investigated by Sewall et. al. [24] that also includes a stationary 180deg bend [20]. Zhang [25] and Liu [26] studied triangular ducts, with and without effects of rotation both experimentally and numerically with various hybrid approaches.

1.2   Aims of the study

The aim of the current work is to extend the bank of existing studies of the SST – SAS model on industrial internal cooling passage flows, providing more detailed numerical insights into the model and quantify its resolving capability further with two-point correlations and energy spectra. Another aim is to test whether the artificial forcing addresses the deficiencies of the SAS found in previous works and establish forcing suitability for the present engineering application.

2.0   NUMERICAL METHODS

2.1   Numerical details

Two solvers were used to obtain the present results: ANSYS Fluent v17.2 and ANSYS CFX v17.2. The simulations without artificial forcing were performed in ANSYS Fluent using the incompressible Finite Volume cell-centred solver with implicit bounded second order time formulation. The Semi-Implicit Method for Pressure Linked Equations (SIMPLE) was used for pressure-velocity coupling. No upwind (smoothing) method was used and all equations were spatially discretised with 2nd order formulations. The bounded second order modification was used for momentum equations as it was found to produce more realistic results and was also recommended for use with the SST – SAS model [11].

Simulations including the forcing were performed in ANSYS CFX with an incompressible finite element-based finite volume formulation and a vertex-based discretisation strategy. Rhie-Chow [27] coupling was used for the pressure-velocity link as the pressure and velocity is collocated. All equations were discretised with second order accuracy formulations without special treatment.

The forcing was implemented in ANSYS Fluent 17.2 via the use of User Defined Function, however it was found by testing that ANSYS CFX has a faster and more robust implementation of the forcing and differs from the authors own implementation only in the number of harmonic modes used. For this reason, the latter was used for simulations with forcing.

All simulations were performed on the University of Nottingham HPC and utilised 64 to 112 cores. The time step range used in the simulations for all unsteady models is 0.00014s to 0.00012s for the most refined grid.

This corresponds to mean Courant number of $0.5 - 0.8$ in the critical regions of interest around the ribs and 1.6 in the streamwise centre of the channel, where the $SST - SAS$ model is expected, and observed, to operate in the modelling mode. Small regions with higher courant number exhibited no unsteadiness or turbulence as they were far away from the ribs. After developing the flow for at least three through flows based on mean inlet velocity, arithmetic averaging was performed on the transient data for another three to five through flows minimum.

Convergence was achieved in both solvers by ensuring that the RMS of residuals drops by at least three orders of magnitude after the time step was incremented. This was achieved in $3 - 6$ iterations per time step.

2.2   Turbulence modelling

The primary model used to simulate the high Re, turbulent flow in the present paper was the Shear Stress Transport – Scale Adaptive Simulation ($SST - SAS$). From a mathematical point of view it was the standard $k - \omega$ URANS model with an extra Q_{SAS} term added to the specific turbulence dissipation rate ω equation:

$$Q_{SAS} = \max\left[\zeta_2 \kappa S^2 \left(\frac{L}{L_{vK}}\right)^2 - C\frac{2k}{\sigma_\varphi}\max\left(\frac{|\nabla\omega|^2}{\omega^2}, \frac{|\nabla k|^2}{k^2}\right), 0\right] \qquad (\quad 1\quad)$$

Physically, the model and its functioning is discussed in more detail by the authors previously in [10] as well as by its creators Menter et.al. [8] [28] and various other authors mentioned previously. In essence, the Q_{SAS} is based on ratio of turbulent length scale to the von Karman length scale and is only significant in regions of high strain and unsteadiness. Where the grid is refined sufficiently to resolve the flow as judged by the term, ω is increased, eddy viscosity is lowered and more of the energy spectrum should be resolved. In this case, once the 'resolving mode' is triggered the underlying $k - \omega$ SST formulation begins to act as a subgrid scale model. Eddy viscosity is limited further by the use of the wall adapting local eddy viscosity (WALE) subgrid model.

2.3   Artificial forcing

The forcing term is applied to momentum as well as the kinetic energy equation and is discussed in detail in the original paper by Menter et. al. [11]. Briefly, the forcing reads:

$$F_{mom,i} = \frac{\rho\, u_{f,i}}{\Delta t}; \quad F_k = -0.5\, \frac{\rho u_{f,i}^2}{\Delta t} \qquad (\quad 2\quad)$$

$$u_{f,i} = \vec{u}(\vec{x}, t) = \sqrt{\frac{2}{3}}k\sqrt{\frac{2}{N}}\sum_{p=1}^{N}[p_i^n \cos(arg^n) + q_i^n \sin(arg^n)] \qquad (\quad 3\quad)$$

Where number of modes N is kept at constant 100 throughout the simulation.

$$p_i^n = \varepsilon_{ijk}\, \eta_j^n\, d_k^n \qquad (\quad 4\quad)$$

$$q_i^n = \varepsilon_{ijk}\, \xi_j^n\, d_k^n \qquad (\quad 5\quad)$$

$$arg^n = 2\pi\left(\frac{d_i^n}{L_t} + \frac{\omega^n t}{\tau_t}\right) \qquad (\quad 6\quad)$$

Where L_t and τ_t are the standard length and time scale of modelled turbulence obtained from the $k - \omega$ SST model and $\eta_i^n, \xi_i^n, d_i^n, \omega^n$ are randomly generated and normally distributed numbers with mean φ and standard deviation ψ, denoted as $N(\varphi, \psi)$.

$$\eta_i^n = N(0,1); \quad \xi_i^n = N(0,1); \quad d_i^n = N(0, 0.5); \quad \omega^n = N(1,1) \qquad (\quad 7\quad)$$

On top of this, Nyquist limiter is used on the above to only transfer energy of modes that can actually be resolved by the grid. Δh is maximum cell extent in any direction, $\Delta h = \max(\Delta x, \Delta y, \Delta z)$

$$\frac{\tau_t}{\omega^n} \geq 2\,\Delta t; \qquad \frac{L_t}{|d^n|} \geq 2\Delta h \qquad\qquad (\ \ 8\ \ )$$

The forcing was applied locally in the specified region on Figure 2a. The forcing can be applied zonally or globally and is only significant in the first few timesteps of the simulation and diminishes with time as the equations move towards more resolved content and a dynamic balance between forcing and the main SAS model develops. If applied zonally, no special treatment at interfaces is necessary with the use of SST – SAS model and it is one of its core advantages as the same model is used inside and outside of the forcing zone. When forcing is applied globally, the SST-SAS model will simply damp it out in the steady regions. If the forcing is to be used with other models such as DES or other hybrid RANS-LES methods it is expected that some treatment at the forcing zone interface would be necessary to ensure correct energy transfer from modelled to resolved zone.

The forcing formulation has been calibrated with spectral data from experiments of Comte-Bellot & Corrsin [29]. A major strength of the spectral forcing is that it transfers the transient energy correctly only based on the modelled length and time scale of turbulence coming from a turbulence model and the velocity field imposed is guaranteed to be divergence free as opposed to the Vortex Method (VM), as explained in Mathey et. al. [30]. VM needs a reasonable initial input to work correctly and divergence-free field is not guaranteed. The inhomogeneity and anisotropy of generated turbulence is also not expressed explicitly in VM, which is the case in the spectral method. The spectral method is therefore preferred.

2.4   Two-point correlations and energy spectra
Two-point correlations and energy spectra are employed motivated by the fact that standard resolved to modelled TKE or Reynolds stresses ratio appears to be insufficient in some cases as demonstrated by Davidson [31]. It was found in the paper by Davidson that even while the resolved to total quantities ratios were over 85% on all grids, some simulations failed to meet the requirements for a well resolved LES. This was only revealed by further inspection of two-point correlations and energy spectra.

If A and B are different points in space, at the same time-step, the standard two-point correlation is defined as:

$$R_{AB}(\vec{r}) = \ <u'(\overrightarrow{x_A})u'(\overrightarrow{x_A} - \vec{r})>\ \qquad\qquad (\ \ 9\ \ )$$

The normalised Welch's power spectral density estimate is used [32] for energy spectra.

3.0   COMPUTATIONAL SETUP

3.1   Geometry and grid
The geometry consists of a development section with eight equi-spaced ribs and a longer outflow region, as shown in Figure 1a. The channel edge is taken as the hydraulic diameter. The square rib height to hydraulic diameter ratio is 0.1 and pitch to rib ratio is 10. The inflow is positioned at half a rib pitch upstream of the first rib and the outflow boundary is sufficiently coarse and far downstream for all the generated recirculation to be dissipated before exiting.
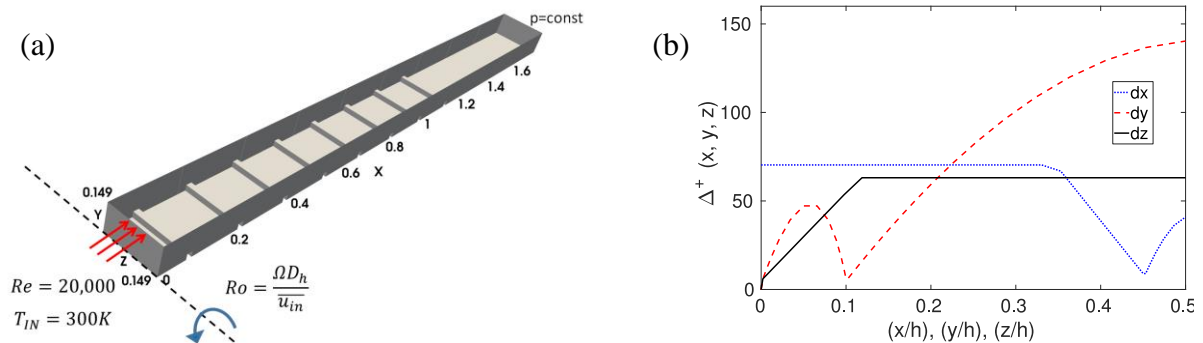

Figure 1 – 3D representation of the geometry, only lower mirrored half is shown. For simulations including rotation, the axis of revolution is always the z-axis with the right-hand rule to determine direction

The grid used in the present study is similar to Viswanathan et.al. [21] and is suitable for DES simulations as shown in Figure 1b and as described by Spalart et. al. [33]. The non-dimensional wall distance y^+ is less than 1.5 in the near-rib region in all cases and varies locally up to $y^+ \cong 4$ The motivation for using the present grid was to test the SST – SAS model on a DES grid and benchmark its resolving performance against DES. From the present simulations, SAS required approximately 15% more computational time than LES and 5% more than DES per iteration on the same grid. If the grid must be refined to LES requirements, the LES approach is more advantageous as it is faster and already proven to produce good results [19]. The study therefore should be beneficial to industrial users of the model as it assesses SST – SAS performance under realistic, cost-efficiency driven environment where grids must be coarse and run times kept to minimum.
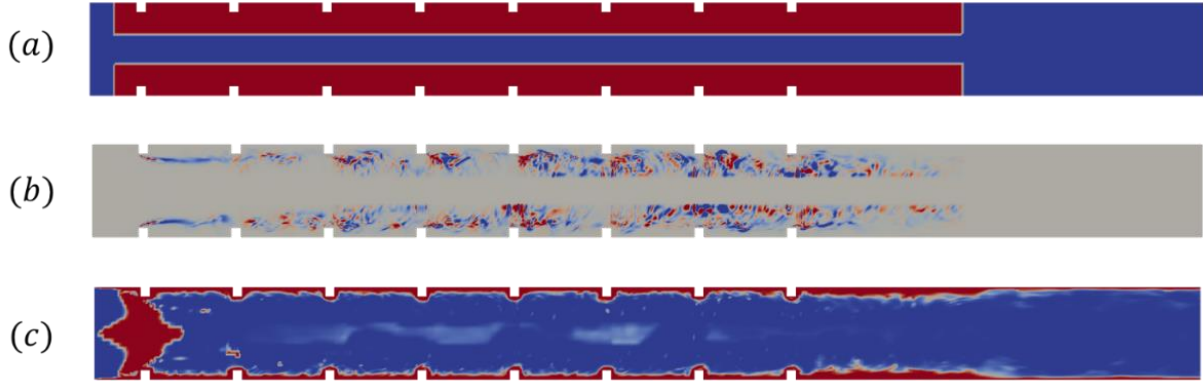

Figure 2 - contour plots showing where the forcing terms are active. (a) is the prescribed area where forcing terms were active in the simulation, (b) is magnitude of the source forcing terms and (c) is the $k - \omega\ SST$ first blending function F1 magnitude indicating modelled near wall region

3.2   Boundary Conditions

The Reynolds number used in the present study is 20,000 based on the hydraulic diameter. The Prandtl number is 0.7 and the Rotation number is 0.3 for the case with rotation examined in the later section. The inlet definition is a constant 'plug flow' definition, as described in experimental following Sewall et. al. [19]. In the numerical simulations of [19] it was found in the paper that imposing a non-constant velocity inlet is inconsequential after the second rib and very minor after the first. A constant velocity inlet was used for simplicity but also to be consistent with other numerical results. It is also shown by Davidson et. al. [9] who performed SST – SAS simulations with a fluctuating, realistic inlet without forcing that it seemed to have very little effect on the solution. This is likely due to the fluctuations being insufficient to switch the SAS model to resolving mode and hence being damped out. Finally, in the LES simulations of Tyacke and Tucker [3] of the same geometry it was also found that turbulent inlet fluctuations of 10% did not have a strong impact on the flow development.

All the walls are prescribed a temperature of 330K, while the inflow temperature is 300K. This latter value is also used as reference in the calculations. Both heat flux and temperature thermal boundary conditions were tried and it was found that very minor differences in heat transfer predictions were observed. Hence the isothermal wall boundary conditions were used for consistency with other available numerical data.

All heat transfer plots are normalised with the hydraulic diameter D_h and Dittus-Boelter correlation:

$$Nu_0 = \ 0.023\ Re_b^{0.8}Pr^{0.4} \qquad\qquad (\quad 10\quad)$$

3.3   SAS Grid investigation

A grid refinement study was performed using the steady state $k - \omega\ SST$ model and the SST-SAS model. While in general a resolving simulation such as SAS is expected to exhibit grid sensitivity as it is tends to DNS with grid refinement, it is still of value to examine the solution sensitivity to the grid.

As shown on Figure 3, without introducing any forcing terms, the transient SST – SAS simulation performed similarly to RANS on the refined grid (approximately $0.5\Delta x$ in any direction). The grid is of LES requirements and has 9.3m cells. Even with such refinement there appears to be very little resolved content.
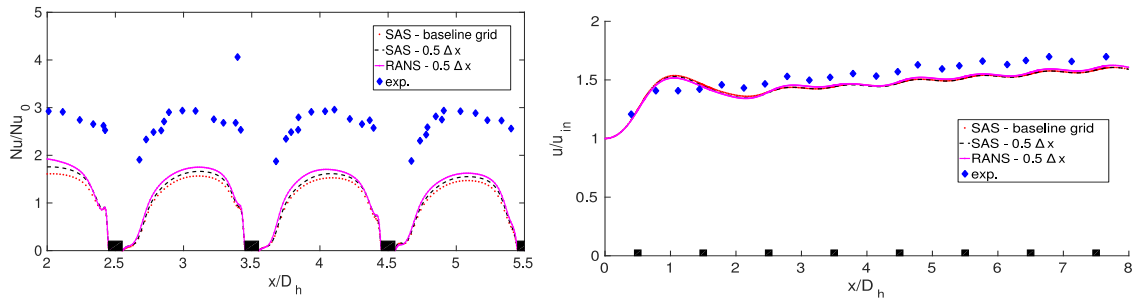
Figure 3 – grid refinement test for SST − SAS model without forcing. RANS solution is tested to be grid-independent.

The figure demonstrates that unforced SST − SAS solution is nearly identical to RANS even with significant grid refinement. In addition very little instantaneous fluctuations were present in the transient SAS solution without forcing. This is indeed the reason for the present work. All unsteady simulations in the present study were started from a well-developed DES solution that exhibited much higher instantaneous unsteadiness than SAS. The final grid used was one consisting of 2.4m cells.

4.0   RESULTS

4.1   Stationary flow

As shown on Figure 4, the forcing appears to make significant difference for the SST − SAS model. The plots show that switching from modelling mode to resolving mode is present when the forcing terms are active. Importantly, unsteady content appears outside the boundary of the forcing zone, suggesting the turbulence is self-sustaining and the entire domain does not need to have the forcing applied. On the other hand, by further examination of the forcing function effect on Figure 2 and Figure 4 it was found that forcing is only significant in the unsteady recirculating regions behind each of the ribs and away from the wall. It is concluded that the forcing could likely be safely applied to the entire domain as it will interact with the SST − SAS model and reduce itself in steady or near-wall regions.
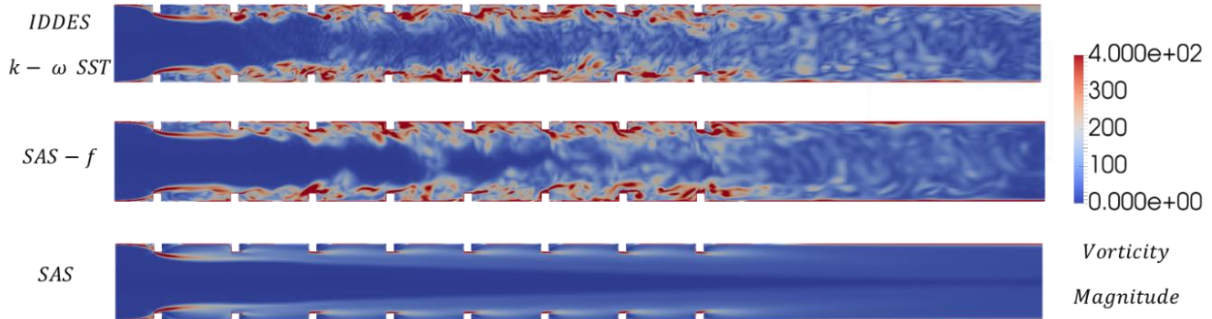

Figure 4 –instantaneous vorticity magnitude at the last time step after at least ten through flows of development. Except for the forcing, grid, boundary conditions and numerical setup are identical for all simulations.

Looking at Q criterion isosurfaces on Figure 5, the absolute magnitude of the Q criterion is not of primary importance, rather it is a useful metric in visualising turbulence. It is again clear from the figure that very little unsteadiness is present in the unforced SST − SAS solution and there is noticeable increase of unsteady content only as a result of the introduction of the forcing terms with identical boundary conditions.

Next, mean velocity profiles and their fluctuations are analysed. Measurements at four locations downstream of the inflow plane are shown on Figure 6. The velocity profiles are taken midway between the ribs in the streamwise direction and midway between the walls in the spanwise direction. The measurement locations in the wall-normal direction range from the $y = 0$ to one quarter of the height of the duct. Apart from the first profile location, an improvement of streamwise velocity prediction is observed with the introduction of the SAS forcing term compared with the original SAS approach. It can also be seen that the profiles are very similar to both the SA and $k − \omega\ SST$ variants of DES.
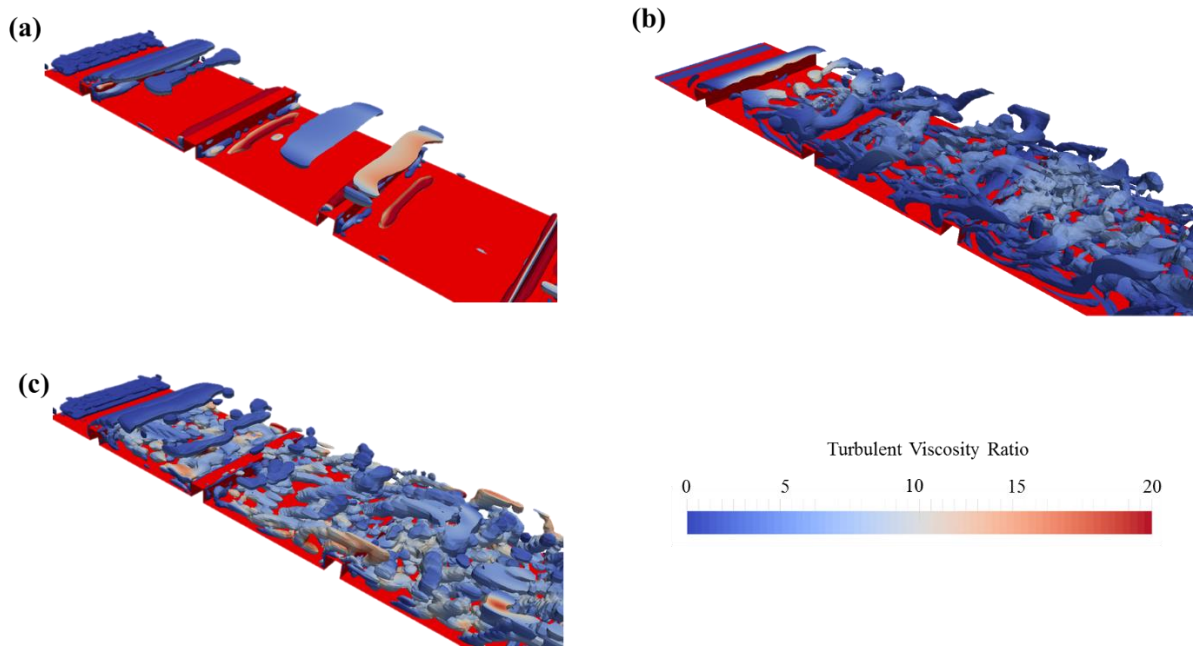
Figure 5 – Normalised Q criterion isosurfaces of 0.2 value coloured by Turbulent Viscosity Ratio. (a) $SST-SAS$ without forcing, (b) $SST-SAS$ with forcing, (c) IDDES $k - \omega\ SST$. Note low eddy viscosity in the unsteady regions.

The velocity fluctuations on Figure 6 in the streamwise direction are both underpredicted and over predicted by all models. The SAS-F model dramatically over predicts the fluctuations at the second profile location and at larger values of y/D_h for the third profile location. At the fourth rib it can be seen that the SAS-F and DES variants are similar. It should be noted that very little resolved turbulence was observed for the standard SAS model as can be seen on the plots. The wall normal velocity fluctuations are generally under predicted by all models and interestingly the values predicted by the SAS-F model are approximately 50% below the DES.
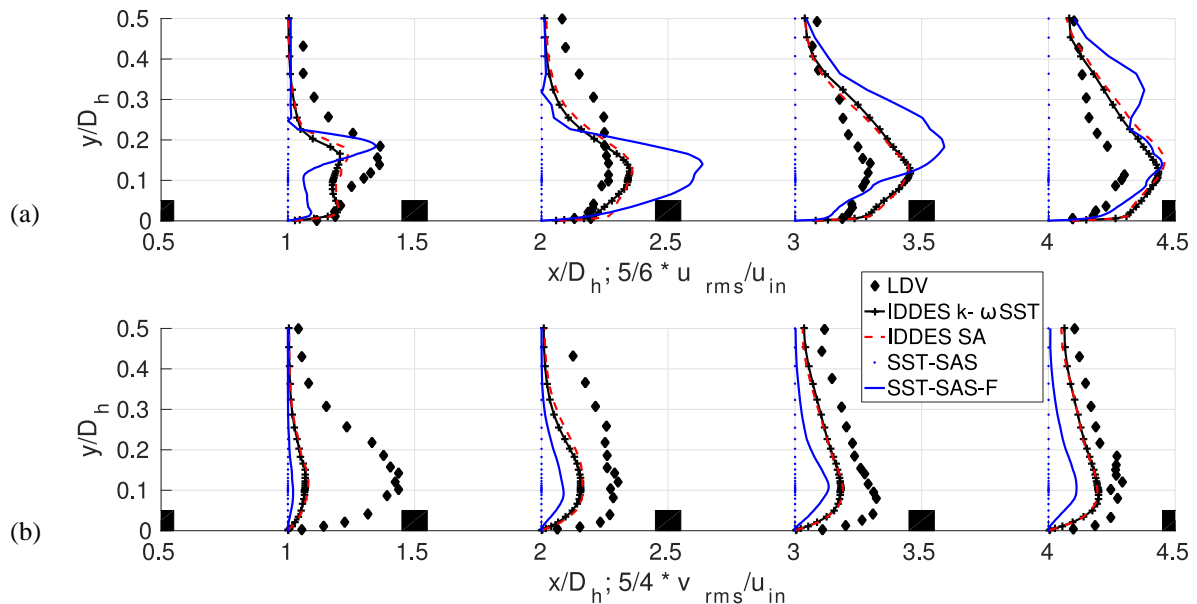

Figure 6 – (a) resolved streamwise and (b) wall-normal fluctuations starting from one rib pitch downstream of inflow plane

To further confirm that the models are operating in resolving mode, ratio of resolved to total turbulent kinetic energy γ is plotted in Figure 7. The ratios are nearly identical after the first rib and arithmetic average of γ for all ribs ahead of the first one was taken for simplicity. Pope [34] recommends that at least 80% of energy should be resolved for a simulation to be considered well-resolved. Apart from the region immediately downstream of the first rib this is true for both DES and SST-SAS. Again it can be seen from the figure that very little resolved turbulent kinetic energy is present in unforced SST-SAS model.
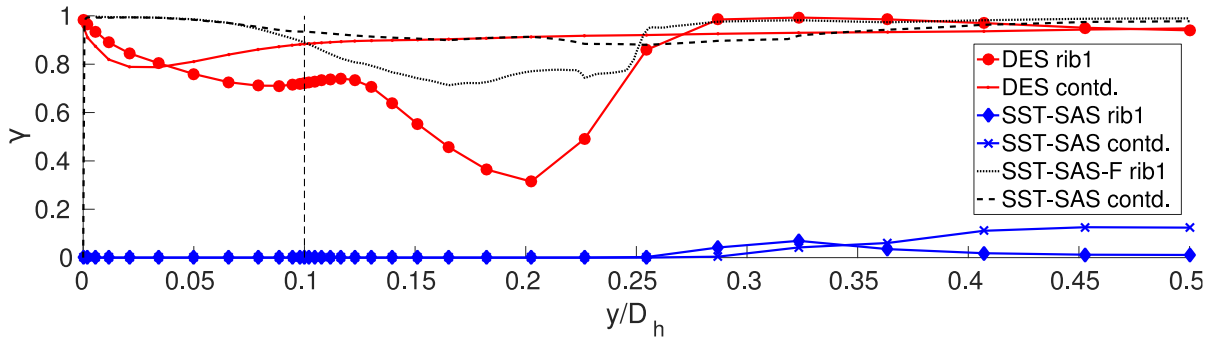
Figure 7 – resolved to total Turbulent Kinetic Energy ratio γ. Locations are the same as previously. The dashed vertical line marks height of the ribs. The plots for ribs 2 and beyond are compounded in a 'continued' plot as they do not vary greatly.

Figure 8 shows the normalised Nu plot along the wall centreline of the channel. The forced SST-SAS solution is significantly improved with respect to RANS. Importantly, the unforced SST-SAS as well as RANS do not predict the sharp peak of cooling efficiency immediately ahead of the ribs and significantly under-predict heat transfer in all cases. The trends themselves predicted by SST-SAS-F and DES are similar to experimentally found ones however the Nusselt number is still significantly underpredicted by all approaches. This suggests deficiency in the near-wall RANS model and that further investigation is required.

Comparing with other authors, the LES of Sewall et.al. [19] is very close to the experimental measurements; the LES predictions are far superior to any other RANS or hybrid RANS-LES performed on the geometry. The hybrid LES-RANS of Tyacke and Tucker [3] is somewhat further away from the experimental solution, but requires significantly less computational effort due to RANS modelling near the wall. Viswanathan and Tafti [21] performed DES and confirmed the present conclusions that DES is much less accurate than LES on the present geometry. They also show that LES exhibits much smaller scale structures than DES, as expected.

Figure 9 shows the energy spectra present in the resolving simulations. It should be noted that such plots were generated at various points behind different ribs and all produced very similar results. The standard SST-SAS model is steady and not shown on this plot. For the SAS-F and DES approaches an inertial range is visible beyond which there is a frequency band indicating the existence of an inertial sub-range with a -5/3 slope. The steeper slope beyond this relates to the damping of the energy content of the frequencies due to molecular and turbulent viscosity. Also shown on the plot is the grid cut-off frequency of 320Hz beyond which structures cannot be resolved. Comparing the forced SST-SAS solution with DES, the low frequency eddies for the SAS-F solution contain more energy and the higher frequency eddies less energy than for DES (close to the cut-off frequency).
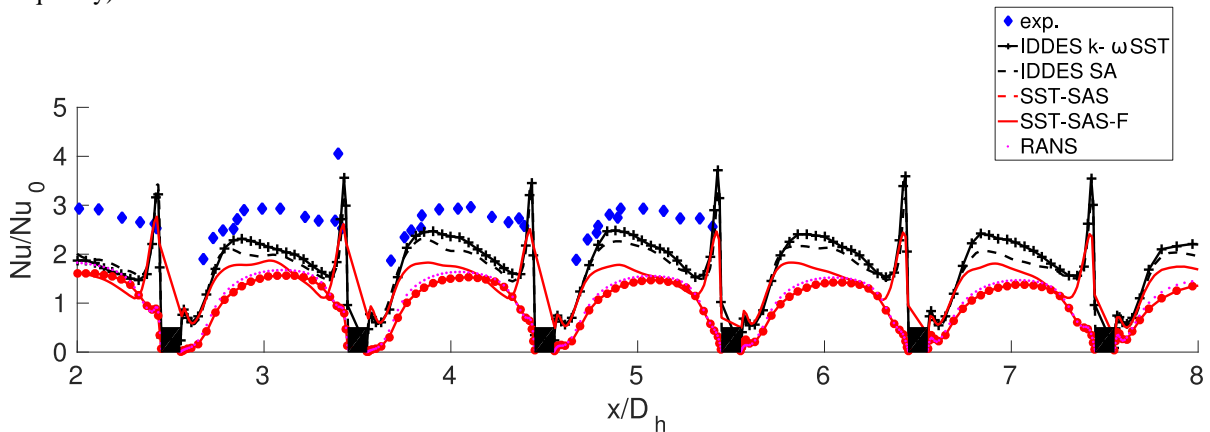

Figure 8- heat transfer measurements and predictions along the wall centreline

Figure 10 shows streamwise and spanwise two-point cross-correlation plots respectively for SAS-F and DES behind the third rib. The SAS-F results show steeper curves and this would indicate that smaller scale structures are more prevalent in downstream grid locations. The correlation plots are generally smoother for forced SAS solution. As expected, the unforced SAS solution exhibits large scale structures only and two point correlations were not obtained as it is essentially a steady solution.
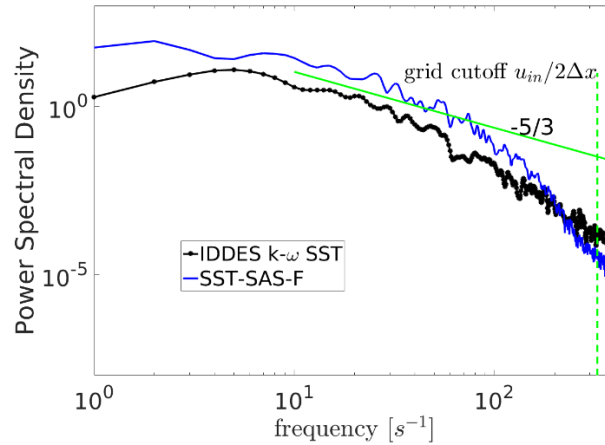
Figure 9 – power spectral density for the models tested. The point is located 10mm downstream of 5th rib, one rib height away from the walls and on the z-midplane. The energy spectrum does not appear to be sensitive to location of the point
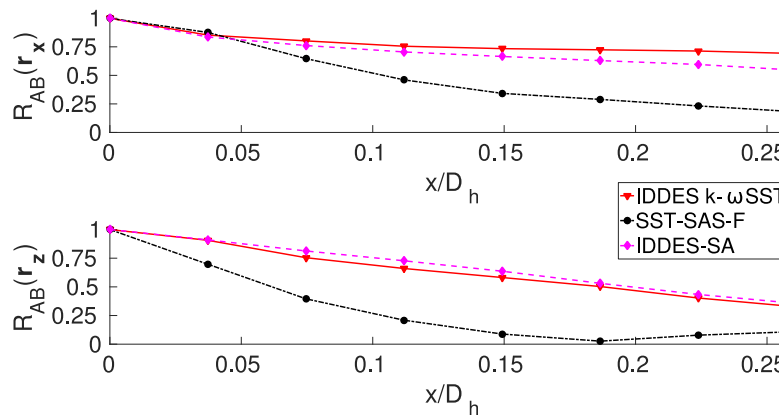

Figure 10 – two-point correlation plots. Approximately 5.56mm spacing between the measurement points. The streamwise lines are located in the centre of the channel in z-normal direction and at one rib height in y-direction. Spanwise lines are located two rib heights behind the rib and level with streamwise ones. Grid spacing varies from 2mm to 4mm along the lines.

4.2   Rotating Flow

In this preliminary work, a Rotation number of 0.3 was used, which corresponds to 37.3 revolutions per minute, with axis of rotation as shown on Figure 1. With added rotations, other boundary conditions are unchanged from the stationary case and similar to LES of Sewall et.al. [24]. Effects of rotation on present type of geometry were also investigated via DES and URANS by Saha et.al. [4]. Experiments were performed by Hibbs et.al. [35]. The following simulations are performed without any additional forcing terms and original SST-SAS formulation.
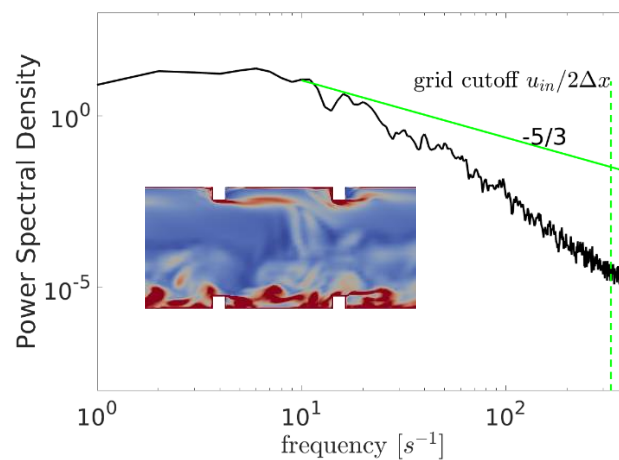

Figure 11 – Power Spectral Density predicted by the original SST-SAS model with effects of rotation. Contours are of vorticity magnitude at the last time step of simulation for fifth and sixth rib.

From Figures 11 and 12 it can be seen that the solution appears unsteady with a much more realistic energy spectrum even though no forcing terms are active. This confirms the findings of Dobrzynski et.al. [36], who used the unforced SST-SAS model on a cavity flow with rotation and obtained results close to experimental measurements. Figure 12 further confirms those observations by comparison with experimental data.
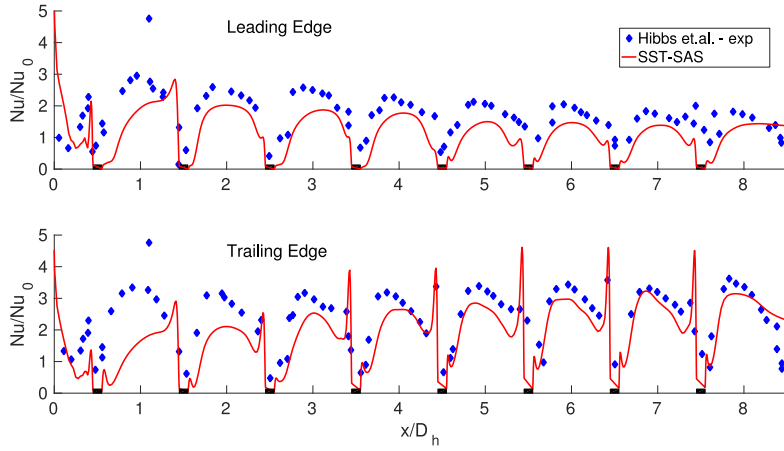

Figure 12 –Heat Transfer predicted by the original SST-SAS model with effects of rotation
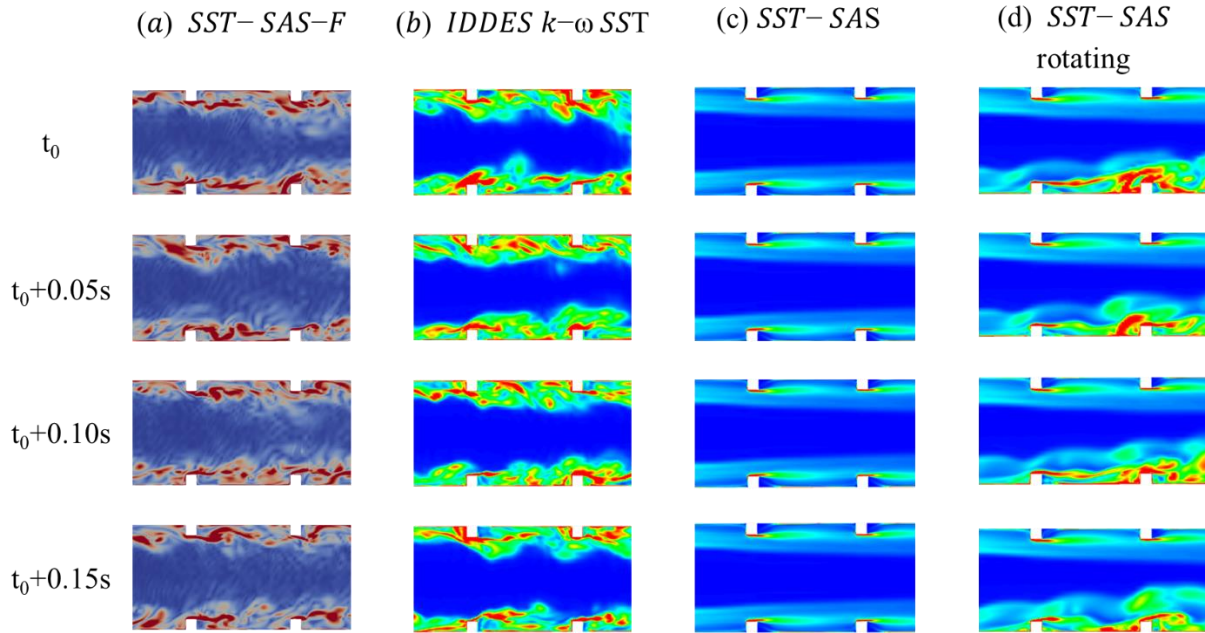

Figure 13 – Time snapshots of vorticity magnitude for the second and third rib. The nitial time varies between the models but is always at least 10 through flows. Time step was 0.00014s in all cases.

To summarise and compare the findings, Figure 13 shows time snapshots of the flow in intervals of 357 time steps for the different models investigated. The figure shows that unforced SAS solution is essentially steady and does not vary with time. For the case with rotation, the SAS model appears to only be resolving the trailing edge, while leading edge appears as URANS. This is consistent with the expectation that rotation causes turbulence to be attenuated at leading edge and amplified at trailing edge. The forced SAS solution seems to exhibit finer turbulent structures than DES.

5.0   CONCLUSIONS

It was confirmed that the SST-SAS model based on the $k - \omega\ SST$ formulation continues to behave as URANS even on a LES-like grid and strongly unsteady flow present at internal cooling related geometry. With stationary flow the introduction of the forcing terms triggers the resolving capability of the model and the solution is significantly improved, including more realistic spectral content. While the solution is still further away from

experiment than DES or LES, it presents a significant improvement over pure SST-SAS. The forcing terms successfully trigger resolving mode with only the modelled time and length scale provided by the base model.

Introducing rotation to the flow seems to trigger the resolving mode of the SAS model similar to that of the SAS-F for the stationary case. This suggests that strong three-dimensionality of the flow is needed to fully make use of the models' benefits.

Future recommendations include further comparisons of rotating flow against other hybrid RANS-LES models. Friction factors and other more detailed metrics of the flow can also be investigated to further assess applicability of SST-SAS. Test cases where DES struggles to obtain accurate solutions are recommended.

ACKNOWLEDGMENTS

REFERENCES

[1]   Boeing inc., "Current Market Outlook 2016-2035," 2016.

[2]   C. Orozco-Pineiro, "ERICKA Project final report," Rolls-Royce Derby, 2014.

[3]   J. Tyacke and P. G. Tucker, "Large eddy simulation of turbine internal cooling ducts," *Comput. Fluids*, vol. 114, pp. 130–140, 2015.

[4]   K. Saha and S. Acharya, "Flow and Heat Transfer in an Internally Ribbed Duct With Rotation: An Assessment of LES and URANS," *ASME Conf. Proc.*, vol. 2003, pp. 481–495, 2003.

[5]   J. Tyacke *et al.*, "LES for Turbines: Methodologies, Cost and Future Outlooks," *J. Turbomach.*, vol. 136, 2013.

[6]   J. C. Tyacke and P. G. Tucker, "Future use of Large Eddy Simulation in Aeroengines," *J. Turbomach.*, vol. 137, 2015.

[7]   U. Piomelli, "Large eddy simulations in 2030 and beyond," *Phil. Trans. R. Soc. A*, vol. 372, no. 20130320, 2014.

[8]   Y. Egorov and F. Menter, "Development and application of SST-SAS turbulence model in the DESIDER project," in *Notes on Numerical Fluid Mechanics and Multidisciplinary Design*, 2008, vol. 97, pp. 261–270.

[9]   L. Davidson, "Evaluation of the SST-SAS model: Channel flow, asymmetric diffuser and axi-symmetric hill," *Eur. Conf. Comput. Fluid Dyn. (ECCOMAS CFD)*, pp. 1–20, 2006.

[10]   P. Zacharzewski, K. Simmons, R. Jefferson-Loveday, and L. Capone, "Evaluation of the sst-sas model for prediction of separated flow inside turbine internal cooling passages," in *Proceedings of the ASME Turbo Expo, GT2016-56117*, 2016.

[11]   F. R. Menter, A. Garbaruk, P. Smirnov, D. Cokljat, and F. Mathey, "Scale-adaptive simulation with artificial forcing," *Notes Numer. Fluid Mech. Multidiscip. Des.*, vol. 111, pp. 235–246, 2010.

[12]   R. H. Kraichnan, "Diffusion by a Random Velocity Field," *Phys. Fluids*, vol. 13, no. 1, p. 22, 1970.

[13]   a. Smirnov, S. Shi, and I. Celik, "Random Flow Generation Technique for Large Eddy Simulations and Particle-Dynamics Modeling," *J. Fluids Eng.*, vol. 123, no. 2, p. 359, 2001.

[14]   A. Keating and U. Piomelli, "Synthetic Generation of Inflow Velocities for Large-Eddy Simulation," *34th AIAA Fluid Dyn. Conf. Exhib.*, pp. 1–13, 2004.

[15]   P. Dhopade, L. Capone, M. Mcgilvray, D. Gillespie, and P. Ireland, "Numerical Modelling Techniques for Turbine Blade Internal Cooling Passages," in *ASME Turbo Expo*, 2015, pp. 1–13.

[16]   D. R. H. Gillespie, J. C. Ryley, and M. Mcgilvray, "Stationary Internal Cooling Passage Experiments for an Engine Realistic Configuration," *Osney Thermo-Fluids Lab*, pp. 1–10, 2011.

[17]   M. Schüler, S. O. Neumann, and B. Weigand, "Experimental investigations of pressure loss and heat transfer in a 180° bend of a ribbed two-pass internal cooling channel with engine-similar cross-sections," *Proc. Inst. Mech. Eng. Part A (Journal Power Energy)*, vol. 223, pp. 709–719, 2009.

[18]   M. Schüler, S. O. Neumann, and B. Weigand, "Numerical investigations of pressure loss and heat transfer in a 180° bend of a ribbed two-pass internal cooling channel with engine-similar cross-sections," *Proc. Inst. Mech. Eng. Part A (Journal Power Energy)*, vol. 224, no. 3, pp. 349–361, 2010.

[19]   E. A. Sewall, D. K. Tafti, A. B. Graham, and K. A. Thole, "Experimental validation of large eddy simulations of flow and heat transfer in a stationary ribbed duct," *Int. J. Heat Fluid Flow*, vol. 27, no. 2, pp. 243–258, 2006.

[20]   E. Sewall, D. Tafti, "Large Eddy Simulation of Flow and Heat Transfer in the 180 deg bend region of a stationary gas turbine blade ribbed internal cooling duct," *J. Turbomach.*, vol. 128, pp. 763–771, 2006.

[21] A. K. Viswanathan and D. K. Tafti, "Detached eddy simulation of turbulent flow and heat transfer in a two-pass internal cooling duct," *Int. J. Heat Fluid Flow*, vol. 27, no. 1, pp. 1–20, 2006.

[22] Y. Liu, "Numerical Simulations Unsteady of Complex Geometry Flows," University of Warwick, 2004.

[23] A. Ooi, G. Iaccarino, P. A. Durbin, and M. Behnia, "Reynolds averaged simulation of flow and heat transfer in ribbed ducts," *Int. J. Heat Fluid Flow*, vol. 23, no. 6, pp. 750–757, 2002.

[24] E. A. Sewall and D. K. Tafti, "Large Eddy Simulation of the Developing Region of a Rotating Ribbed Internal Turbine Blade Cooling Channel," *ASME Conf. Proc.*, vol. 2004, no. 41685, pp. 735–747, 2004.

[25] Y. M. Zhang, W. Z. Gu, and J. C. Han, "Augmented heat transfer in triangular ducts with full and partial ribbed walls," *J. Thermophys. Heat Transf.*, vol. 8, no. 3, pp. 574–579, 1994.

[26] Y.-H. Liu, M. Huh, J.-C. Han, and H.-K. Moon, "High Rotation Number Effect on Heat Transfer in a Triangular Channel With 45[degree], Inverted 45[degree], and 90[degree] Ribs," *ASME Conf. Proc.*, vol. 2009, no. 48845, pp. 127–138, 2009.

[27] W. L. Rhie, C.M and Chow, "'Numerical Study of the Turbulent Flow Past an Airfoil with Trailing Edge Separation.,'" *AIAA J. 21*, vol. 11, no. 11, pp. 1525–1532, 1983.

[28] F. R. Menter and Y. Egorov, "Formulation of the Scale-Adaptive Simulation (SAS) Model during the DESIDER Project," *DESider - A Eur. Effort Hybrid RANS-LES Model.*, pp. 51–62, 2009.

[29] G. Comte-Bellot and S. Corrsin, "The use of a contraction to improve the isotropy of grid-generated turbulence," *J. Fluid Mech.*, vol. 25, no. 4, p. 657, 1966.

[30] F. Mathey, D. Cokljat, J. P. Bertoglio, and E. Sergent, "Assessment of the vortex method for Large Eddy Simulation inlet conditions," *Prog. Comput. Fluid Dyn.*, vol. 6, pp. 58–67, 2006.

[31] L. Davidson, "Large Eddy Simulations: How to evaluate resolution," *Int. J. Heat Fluid Flow*, vol. 30, no. 5, pp. 1016–1025, 2009.

[32] P. D. Welch, "The Use of Fast Fourier Transform for the Estimation of Power Spectra: A Method Based on Time Averaging Over Short, Modified Periodograms," *IEEE Trans. Audio Electroacoust.*, vol. 15, no. 2, pp. 70–73, 1967.

[33] R. Spalart, "Young-Person's Guide Simulation Grids Detached-Eddy," *NASA Tech. Note*, vol. 211032, no. July, pp. 1003–1008, 2001.

[34] S. B. Pope, "Turbulent Flows.pdf." 2000.

[35] R. G. Hibbs, S. Acharya, Y. Chen, and D. E. Nikitopoulos, *Heat/mass transfer distribution in a rotating, two-pass channel with smooth and ribbed walls*. New York, NY: ASME, 1996.

[36] A. Szymanski and S. Dykas, "Unsteady flow field evaluation in labyrinth seals by means of computational fluid dynamics," pp. 76–85, 2016.